DALTON
FULL PAPER

Synthesis and characterisation of dimanganese(III) complexes of 1,5-bis(X-salicylidenamino)pentan-3-ol (X = 3- or 5-methoxy) and their catalytic activity towards hydrogen peroxide disproportionation †

Claudia Palopoli,[a] Manuel González-Sierra,[b] Gustavo Robles,[a] Françoise Dahan,[c] Jean-Pierre Tuchagues[c] and Sandra Signorella*[a]

[a] *Departamento de Química, Facultad de Ciencias Bioquímicas y Farmacéuticas, UNR, Suipacha 531, 2000 Rosario, Argentina. E-mail: signorel@infovia.com.ar*
[b] *Instituto de Química Orgánica de Síntesis (IQUIOS), CONICET – UNR, Suipacha 531, 2000 Rosario, Argentina*
[c] *Laboratoire de Chimie de Coordination du CNRS, UPR 8241, 205 Route de Narbonne, 31077 Toulouse Cedex, France*

Received 13th May 2002, Accepted 2nd September 2002
First published as an Advance Article on the web 17th September 2002

Structural, magnetic, electrochemical, EPR, ^{1}H NMR, and H_2O_2 reactivity studies are reported for $[Mn^{III}_2$(X-salpentO)(μ-AcO)(μ-MeO)$(MeOH)_2]$Br (**1**: X = 5-OMe and **2**: X = 3-OMe; salpentOH = 1,5-bis(salicylidenamino)pentan-3-ol). The X-ray diffraction analysis of **2** reveals that the manganese atoms possess an axially elongated-octahedral geometry. The elongation is perpendicular to the bridging plane resulting in a short Mn ··· Mn distance of 2.9278(6) Å. The ligand lies in the meridional plane and the sixth co-ordination position of each manganese atom is occupied by a methanol molecule providing two substitution-labile sites in *cis*-position. Solution structural studies indicate that complexes **1** and **2** are stable in methanol and dmf, even in the presence of water, and the solid state structure is retained in solution. The two complexes show catalytic activity toward disproportionation of H_2O_2 in methanol and dmf at 25 °C. The initial rate of oxygen evolution in the presence of **1** or **2** is first order in [catalyst] and show saturation kinetics with $[H_2O_2]$. Complexes **1** and **2** dismutate H_2O_2 without a kinetic lag phase and are implicated as the active form of the reduced catalyst. Comparison to other dimanganese complexes of this family reveals that the methoxy phenyl-ring substituted derivatives are more effective at reducing H_2O_2 but are less efficient at binding the H_2O_2 substrate (higher K_M) than the 5-bromo or the unsubstituted complexes.

Introduction

Catalases disproportionate intracellular hydrogen peroxide and provide a vital biological defence against this toxic oxygen metabolite. Most catalases contain a heme cofactor; however, nonheme catalases that require manganese as a cofactor[1] have been found from three bacterial origins: *Lactobacillus plantarum*,[2,3] *Thermus thermophilus*[4] and *Thermoleophilum album*.[5] These manganese catalases contain a dimanganese centre and catalyse the disproportionation of hydrogen peroxide into water and molecular oxygen with a catalytic cycle involving transformation between the Mn^{II}_2 and Mn^{III}_2 oxidation states.[6–9] A large number of dinuclear manganese complexes of various types of ligands have been synthesized and structurally characterized and many model complexes have been reported that show catalase activity.[10–16] However, the best chemical mimics of the manganese catalases are 10^3–10^5 slower than the enzymes. The obtention of more effective mimics could find applications as therapeutic agents against oxidative stress and as catalysts for bleaching and organic chemistry[17–19] while also helping to elucidate the features important for the enzymatic mechanisms.

The mechanism of H_2O_2 dismutation has been examined in detail only for a few dimanganese complexes. Among them, dimanganese complexes obtained with a septadentate ligand with benzimidazoyl groups[20,21] and with the 1,3-bis(salicylidenamino)propan-2-ol (salpnOH) ligand and their phenyl-ring substituted derivatives[10,22,23] have been found to disproportionate H_2O_2 with saturation kinetics by cycling between the Mn^{II}_2 and Mn^{III}_2 oxidation states. Two Mn^{III}_2 complexes formed with the higher homologue of salpnOH, 1,5-bis(salicylidenamino)-pentan-3-ol (salpentOH)[24] and its 5-bromo substituted derivative (5-Br-salpentOH),[15] also exhibit saturation kinetics with hydrogen peroxide, although high-valence oxo-manganese species were proposed to be involved in the catalytic cycle.[15] $[Mn_2$(salpentO)(μ-MeO)(μ-AcO)$(MeOH)_2]$Br has been found to possess a higher catalytic rate and a better efficiency to disproportionate hydrogen peroxide than $[Mn_2$(5-Br-salpentO)-(μ-MeO)(μ-AcO)$(MeOH)_2]$Br.[15] This seems to indicate that a more electron-donating substituent could improve the performance of this class of catalysts. In this work, we present the synthesis and characterisation of two new dinuclear Mn^{III} complexes in this series, $[Mn^{III}_2$(X-salpentO)(μ-AcO)(μ-MeO)-$(MeOH)_2]$Br (**1**: X = 5-OMe and **2**: X = 3-OMe), and evaluate their ability to disproportionate hydrogen peroxide as a means to obtain more information regarding the mechanism of H_2O_2 dismutation by this class of complexes.

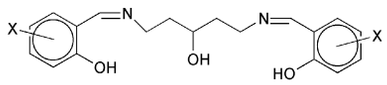

X-salpentOH: X = 5-OMe or 3-OMe

† Electronic supplementary information (ESI) available: ^{1}H NMR spectra of **3** upon addition of sodium benzoate and acetate (Fig. S1); ^{1}H NMR spectra of **1** in basic medium and d_7-dmf (Fig. S2); a plot of the effect of [catalyst] on r_i (Fig. S3) and UV-VIS spectra of the reaction mixture (Figs. S4 and S5). See http://www.rsc.org/suppdata/dt/b2/b204566d/

DOI: 10.1039/b204566d

Results

Structure of [Mn_2(3-OMe-salpentO)(μ-MeO)(μ-AcO)-(MeOH)$_2$]Br (2)

Fig. 1 shows the crystal structure of **2** and selected bond distances and angles are summarized in Table 1. The manganese ions are bridged by the alkoxo oxygen atom of the ligand, one methoxo oxygen atom and one bidentate acetate ligand. The phenolate oxygen, imine nitrogen and alkoxide oxygen atoms of the ligand and the methoxide oxygen atom form a meridional geometry around each Mn, with the sixth co-ordination position of each manganese atom occupied by a methanol molecule. The bromide ion forms hydrogen bonds with H7 and H8 of the co-ordinating methanol molecules. The manganese atoms possess an axially elongated-octahedral geometry. Elongation occurs along the O5–Mn1–O7 and O6–Mn2–O8 axes and is accompanied by compression of the other Mn^{III}–ligand bond lengths, resulting in a short Mn1 ··· Mn2 distance of 2.9278(6) Å. Elongation perpendicular to the bridging plane was also observed for [Mn_2(salpentO)(μ-MeO)(μ-AcO)-(MeOH)$_2$]Br (**3**) and [Mn_2(5-Br-salpentO)(μ-MeO)(μ-AcO)-(MeOH)$_2$]Br (**4**), which posses Mn ··· Mn distances of 2.943(3) and 2.932(1) Å, respectively.[15,24] These Mn ··· Mn distances are shorter than those observed for dialkoxo bridged Mn_2^{III} complexes (3.22–3.24 Å) with a Jahn–Teller elongation axis oriented along the bridging core.[22,23,25]

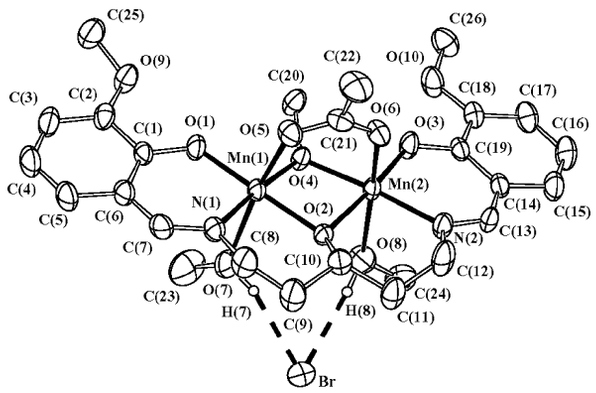

Fig. 1 Asymmetric unit of [Mn_2(3-MeO-salpentO)(μ-MeO)(μ-AcO)-(MeOH)$_2$]Br (**2**) (hydrogen atoms have been omitted for clarity).

Table 1 Selected bond lengths (Å) and angles (°) for [Mn_2(3-MeO-salpentO)(μ-MeO)(μ-AcO)(MeOH)$_2$]Br (**2**)

Mn(1)–O(1)	1.847(2)	Mn(2)–O(3)	1.844(2)
Mn(1)–O(2)	1.935(2)	Mn(2)–O(2)	1.942(2)
Mn(1)–O(4)	1.936(2)	Mn(2)–O(4)	1.939(2)
Mn(1)–O(5)	2.138(2)	Mn(2)–O(6)	2.166(2)
Mn(1)–O(7)	2.327(2)	Mn(2)–O(8)	2.339(2)
Mn(1)–N(1)	2.007(2)	Mn(2)–N(2)	1.999(2)
O(1)–Mn(1)–O(2)	170.53(9)	O(3)–Mn(2)–O(2)	170.62(8)
O(1)–Mn(1)–O(4)	92.02(8)	O(3)–Mn(2)–O(4)	92.30(8)
O(1)–Mn(1)–O(5)	96.49(9)	O(3)–Mn(2)–O(6)	97.94(9)
O(1)–Mn(1)–O(7)	92.28(9)	O(3)–Mn(2)–O(8)	90.48(9)
O(1)–Mn(1)–N(1)	91.82(9)	O(3)–Mn(2)–N(2)	91.64(9)
O(2)–Mn(1)–O(4)	80.03(9)	O(2)–Mn(2)–O(4)	79.78(7)
O(2)–Mn(1)–O(5)	89.04(8)	O(2)–Mn(2)–O(6)	87.47(8)
O(2)–Mn(1)–O(7)	83.03(8)	O(2)–Mn(2)–O(8)	84.54(8)
O(2)–Mn(1)–N(1)	95.83(9)	O(2)–Mn(2)–N(2)	96.08(8)
O(4)–Mn(1)–O(5)	92.58(8)	O(4)–Mn(2)–O(6)	92.35(8)
O(4)–Mn(1)–O(7)	92.57(9)	O(4)–Mn(2)–O(8)	89.90(8)
O(4)–Mn(1)–N(1)	174.85(9)	O(4)–Mn(2)–N(2)	175.42(9)
O(5)–Mn(1)–O(7)	169.66(9)	O(6)–Mn(2)-O(8)	171.18(8)
O(5)–Mn(1)–N(1)	90.41(9)	O(6)–Mn(2)–N(2)	89.41(9)
O(7)–Mn(1)–N(1)	83.84(10)	O(8)–Mn(2)–N(2)	87.74(9)
Mn(1)–O(2)–Mn(2)	98.08(8)	Mn(1)–O(4)–Mn(2)	98.14(8)

Magnetic properties of 2

Solid-state magnetic susceptibility (χ_M) data for **2** were collected in the temperature range 4–300 K and the plots of χ_M and effective magnetic moment (μ_{eff}) against temperature are shown in Fig. 2. μ_{eff} (per dinuclear complex) decreases from 5.85 μ_B at room temperature to 0.75 μ_B at 8 K, indicating an antiferromagnetic coupling of the two Mn^{III} ions of the dinuclear complex. We analysed the temperature dependence of the magnetic susceptibility of complex **2** by employing eqn. (1) derived from the van Vleck equation with the eigenvalues of the isotropic spin-exchange Hamiltonian $H = -2JS_1S_2$ ($S1 = S2 = 2$),[26] modified by including a correction for a paramagnetic monomeric Mn^{III} impurity (eqn. (2)).

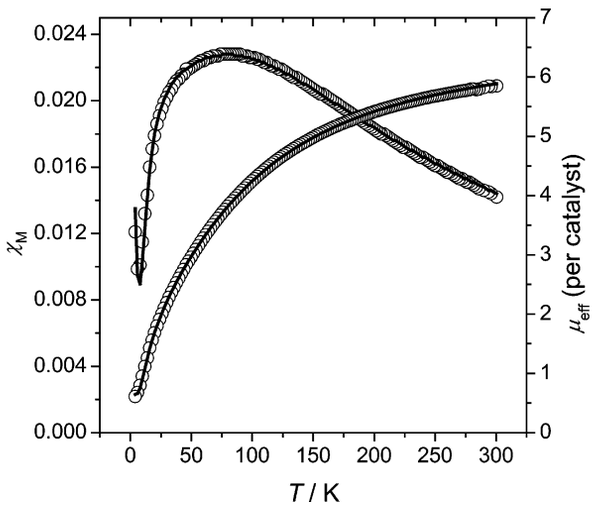

Fig. 2 Variable-temperature magnetic susceptibility data for [Mn_2-(3-MeO-salpentO)(μ-MeO)(μ-AcO)(MeOH)$_2$]Br **2**. Fit lines were calculated using eqn. (2).

$$\chi' = Ng^2\mu_B^2(2e^{2x} + 10e^{6x} + 28e^{12x} + 60e^{20x})/ kT(1 + 3e^{2x} + 5e^{6x} + 7e^{12x} + 9e^{20x}) \quad (1)$$

where χ' is the molar susceptibility and $x = J/kT$

$$\chi_M = (1 - p)\chi' + p\chi_c \quad (2)$$

where χ_M is the total molar susceptibility, χ' is the spin-coupled susceptibility calculated from eqn. (1), χ_c is the Curie law magnetic susceptibility for the monomer and p is the percent of paramagnetic impurity. The least-squares refinements obtained with this model afforded very good fits for the parameters: g = 1.98, J = −13.7 cm^{-1} and p = 1.8 %. Fig. 2 shows the fit to the data for complex **2** based on eqn. (2), for χ_M and μ_{eff}, where μ_{eff} is given by $2.828(\chi T)^{1/2}$. The antiferromagnetic interactions observed for complex **2** have the same order of magnitude as previously observed for other Mn_2^{III} complexes where the bridging alkoxide oxygen atoms are not situated on the individual axes corresponding to the elongation of the co-ordination octahedra.[24,25,27] In this type of complex, the resulting short Mn ··· Mn distance may allow direct overlap between the d_{xy} orbitals, thus providing a plausible exchange mechanism for the antiferromagnetic interaction observed.[25]

Electrochemistry

The cyclic voltammetry of **1** and **2** in methanol (platinum electrode) shows two reduction waves (Fig. 3(a.b)) assigned to the $Mn_2^{III}/Mn_2^{II,III}$ and $Mn_2^{II,III}/Mn_2^{II}$ couples based on coulometry studies. The $Mn_2^{III}/Mn_2^{II,III}$ couple is quasi-reversible and is observed at 52 mV for complex **1** and 84 mV for complex **2**. The $Mn_2^{II,III}/Mn_2^{II}$ couple is non-reversible and is observed around −500 mV for the two complexes and seems to be independent

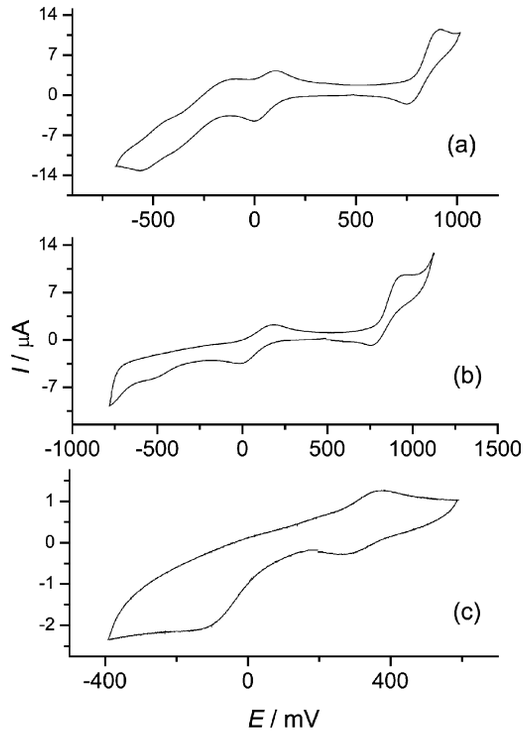

Fig. 3 Cyclic voltammograms of (a) **1** in methanol; (b) **2** in methanol; (c) **1** in dmf. Conditions: Pt/Pt/Ag–AgCl; conc. = 1 mM; scan rate = 100 mV s^{-1}; supporting electrolyte = Bu_4NPF_6.

of the ligand phenyl substituent. In dmf, the cyclic voltammetry of **1** and **2** shows a non-reversible $Mn_2^{III}/Mn_2^{II,III}$ reduction at *ca.* −150 and −180 mV and a quasi-reversible $Mn_2^{III}/Mn_2^{III,IV}$ couple at 319 and 348 mV, respectively (Fig. 3(c)).

The $Mn_2^{III}/Mn^{IV}Mn^{III}$ and $Mn_2^{III}/Mn^{II}Mn^{III}$ redox potentials of complexes in this series are dependent on the electronic properties of the phenyl-ring substituent. Complexes **3**, **4** and $[Mn_2(5\text{-}NO_2\text{-salpentO})(\mu\text{-MeO})(\mu\text{-AcO})(MeOH)_2]Br$ (**5**) undergo a quasi-reversible $Mn_2^{III}/Mn_2^{II,III}$ reduction in methanol at 100, 145 and 255 mV (*vs.* Ag/AgCl), respectively. In dmf, complexes **3** and **4** show a quasi-reversible $Mn_2^{III}/Mn_2^{IV,III}$ couple at 384 and 498 mV (*vs.* Ag/AgCl), respectively. The redox potentials of the two redox processes for the 5-substituted complexes (**1**, **3**–**5**) give linear correlation when plotted against the Hammet substituent parameter, σ_p (Fig. 4). The substituent effect in these complexes may be relayed to the metal ion by two pathways *via* the phenolate and imine groups and the Hammet correlation may result from the combined effect of both pathways. However, the good correlation with σ_p suggests that, for the present complexes, the dominant substituent effect is *via* the phenolate group, as already observed for other series of complexes obtained with Schiff base ligands.[28]

^{1}H NMR

The ^{1}H NMR spectra of **1**, **2** and **3** in d_4-methanol are very simple and indicate a highly symmetrical environment for the Schiff base ligand (Fig. 5 and S1(a)†). The spectra reveal a typical pattern for these complexes, containing a characteristic acetate resonance and distinctive ligand resonances. The paramagnetic shift indicates the presence of weak antiferromagnetic coupling between the Mn^{III} ions in the Mn_2^{III} species. One (**1**) or two (**2**, **3**) resonances are observed between −11 and −21 ppm, which can be assigned to the H4 and H5 protons in accordance with previous studies.[29–31] In the case of **1**, the resonance at −17.87 ppm can be unambiguously assigned to H4, since H5 is replaced by the 5-MeO group in this complex. The protons *ortho* to the donor groups of the Schiff base ligand (H3 and H6) are not observed, and this is consistent with previous findings for Mn^{III} complexes with related bases.[29–31]

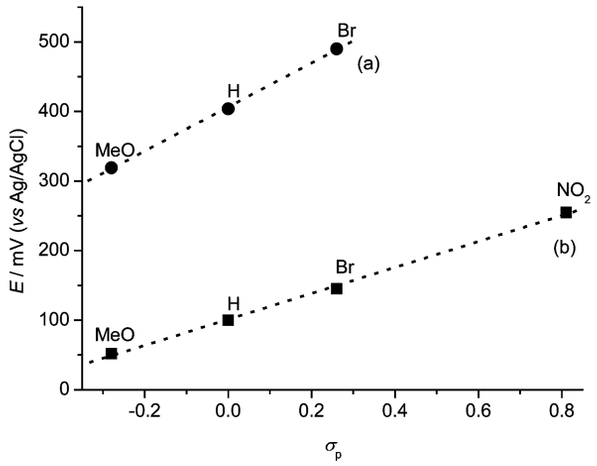

Fig. 4 Hammet plot of redox potentials (*vs.* Ag/AgCl) of complexes **1**–**5** against substituent parameter, σ_p. (a) $Mn_2^{III}/Mn^{III}Mn^{IV}$, in dmf. (b) $Mn_2^{III}/Mn^{II}Mn^{III}$, in methanol.

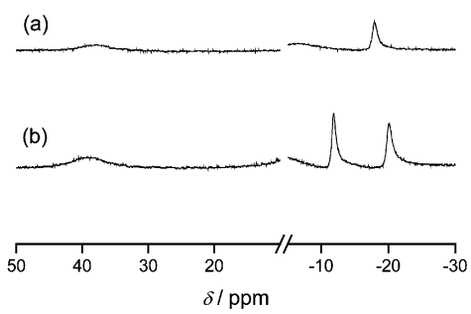

Fig. 5 ^{1}H NMR spectra of (a) **1** and (b) **2**, in d_4-methanol. [catalyst] = 14 mM.

An intense resonance appears at 5.60 ppm (complex **1**) and 5.30 ppm (complex **2**) and can be assigned to the methyl protons of the methoxy substituent on the phenyl-ring, as it is not present in the ^{1}H NMR spectrum of **3**.

The resonance at 38–40 ppm can be assigned to the methyl group of the bridging acetate of **1**–**3** on the basis of its large downfield shift as suggested for other $Mn_2^{III}(\mu\text{-OAc})$ complexes.[32–34] This assignment was confirmed by addition of sodium benzoate to the solution of the complexes in d_4-methanol. The broad signal at 38 ppm (298 K) disappears upon addition of excess benzoate to a methanolic solution of **3** and two new signals at 9.65 and 6.80 ppm corresponding to the benzoate protons appear in the ^{1}H NMR spectrum, together with a new signal at 13 ppm (Fig. S1(b)†). Addition of excess acetate to this solution results in an up-field shift of the 13 ppm signal to 6.5 ppm, while the benzoate protons are now observed at 8.42 and 7.04 ppm (Fig. S1(c)†). In order to determine if the signals observed at 13 (Fig. S1(b)†) and 6.5 ppm (Fig. S1(c)†) correspond to the acetate protons, we examined the effect of adding NaOAc to a methanolic solution of **1**. Indeed, the broad acetate proton resonance moves up-field upon addition of NaOAc to the solution of **1** in d_4-methanol. The shift of the signal is indicative of dynamic averaging resulting from a rapid exchange mechanism between bridging and free acetate. As NaOAc concentration increased from 0.2 to 1.3 equivalents, the signal shifted to lower δ values and sharpened, and a good linear correlation between the chemical shift of the acetate protons and the proportion of free acetate to complex could be established (Fig. 6). This correlation provides a means of quantifying the proportion of the acetate bridged in the Mn_2^{III} complex to free acetate in solution, and is useful to evaluate the recovery of the starting catalyst in the H_2O_2 disproportionation reaction.

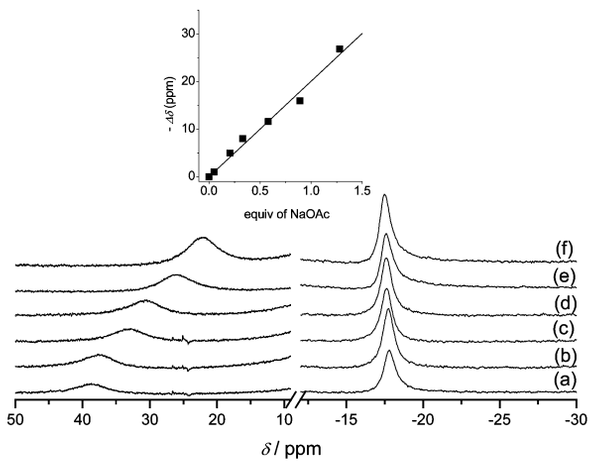

Fig. 6 ^{1}H NMR spectra of **1** (15 mM) after addition of (a) 0.00, (b) 0.05, (c) 0.2, (d) 0.33, (e) 0.6 and (f) 0.9 equiv. of NaOAc, in d_4-methanol.

It has been found that there is a strong linear correlation between the isotropic shift of the acetate protons and the magnetic coupling constant (J) for a number of dinuclear Mn_2^{III} complexes.[32] The observed isotropic shift (38–40 ppm) for the acetate group of complexes **1**–**3** is that expected for bridged acetate Mn_2^{III} complexes with J in the range -15 to -13 cm^{-1} (the calculated J values for **2** and **3**[24] in the solid state are -13.7 and -13.2 cm^{-1}, respectively). This result strongly suggests that the solid-state structure of these complexes is retained in solution.

We used ^{1}H NMR spectroscopy to monitor the complex under catalytic conditions in the presence of H_2O_2. Either a 10-, 50- or 100-fold excess of H_2O_2 was added to three 12 mM samples of **1** in d_4-methanol. Immediately after addition of H_2O_2, oxygen bubbles were observed and the ^{1}H NMR spectra were taken when O_2 evolution had ceased. The spectra showed that the proton resonances from the Schiff base ligand remain unchanged, indicating retention of the complex nuclearity during H_2O_2 disproportionation by **1** in methanol. The ^{1}H NMR spectrum obtained after reaction of **1** with 10 equiv. of H_2O_2 is identical to the initial ^{1}H NMR spectrum of **1**. However, the chemical shift of the bridging acetate protons moved to lower values with increasing [H_2O_2], and this chemical shift was used to determine the percent of catalyst at the end of the disproportionation reaction by employing the correlation determined above. Thus, the proportion of the starting Mn_2^{III} catalyst with the bridging acetate was found to be 93% for the 50 : 1 [H_2O_2] : **1** ratio, which is in accordance with the 8% decrease of the two UV-VIS bands of complex **1** at 410 and 663 nm at the end of the reaction for the same H_2O_2 to **1** ratio. When a 100 : 1 H_2O_2 to catalyst ratio was used, H_2O_2 was completely converted into O_2 and H_2O in a few minutes. However, the ^{1}H NMR spectrum recorded at the end of the reaction revealed the presence of only 65% of the starting complex, in accordance with the spectrophotometric data. Higher [H_2O_2] could not be used because of the strong ^{1}H water signal.

We examined the effect of addition of base on the ^{1}H NMR spectra of **1** in d_4-methanol. The spectrum obtained upon addition of 10 equiv. of NaOMe is shown in Fig. S2(a).†The proton resonances of the ligands now appear in the range for diamagnetic compounds although they are significantly broadened and the chemical shifts differ from those of the free ligand. It is unlikely that paramagnetic impurities cause this broadening, as different batches of this compound yielded exactly the same spectra. Since the size of the isotropic shift reflects the strength of the intermanganese magnetic interaction,[29,34–37] the smaller paramagnetic shift of the ligand protons indicates that the antiferromagnetic coupling between Mn ions is stronger than in **1**. The ^{1}H NMR spectra obtained in basic medium can be interpreted in terms of the formation of an oxo-bridged Mn_2^{III} complex, which should decrease the Mn ··· Mn distance and provide a better exchange pathway between Mn ions. This is consistent with the shift of the phenolate-to-Mn charge-transfer band (of the salpentO ligand) in the UV-VIS absorption spectrum from 410 nm for **1** in methanol to 371 nm (ε = 8700 M^{-1} cm^{-1}) for **1** in basic medium.[38]

Another interesting spectral feature of the spectrum in basic medium is the disappearance of the broad resonance corresponding to the bridging-acetate and the observation of a signal at 1.89 ppm, which can be assigned to the free acetate protons or to a labile monodentate terminal acetate.[34]

The complex generated in basic medium could not be monitored under catalytic conditions in the presence of H_2O_2, because when H_2O_2 is added to the basic solution of **1** a brown precipitate rapidly forms together with vigorous O_2 evolution. Addition of D_2O – the same quantity as introduced when H_2O_2 is added – to the solution of **1** in NaOMe, also causes precipitation of this brown solid, revealing that water is responsible for decomposition of the manganese species generated in this medium.

We have also followed H_2O_2 disproportionation by **1** in d_7-dmf. In this solvent, the resonance of H4 is observed at -15.5 ppm and the bridging acetate protons appear at 37 ppm (Fig. S2(b)†). When a 50-fold excess of H_2O_2 is added to the d_7-dmf solution of **1**, the ^{1}H NMR spectrum of the mixture at the end of O_2 evolution shows the signal at -15.5 ppm but that of the bridging acetate protons disappears. Thus, in this solvent, acetate dissociates completely or converts to a labile monodentate terminal acetate.

Catalytic activity

Stoichiometry. We measured the stoichiometry of the disproportionation of H_2O_2 catalysed by **1** and **2** by volumetric determination of the evolved O_2. In methanol, complexes **1** and **2** quantitatively convert up to 200 equivalents of H_2O_2 to O_2, but the rate of O_2 evolution gradually decreases, and when a new portion of excess H_2O_2 is added to this reaction mixture, the rate of O_2 evolution becomes extremely slow. In dmf, complexes **1** and **2** quantitatively convert over 1500 equiv. of H_2O_2 to O_2. In this solvent, when more than 500 equiv. of H_2O_2 have been consumed, a brown solid appears, meaning that the catalyst partially decomposes. Then, the reaction smoothly decelerates, but the total amount of O_2 evolved corresponds to half the equivalent of H_2O_2 added, indicating that all H_2O_2 disproportionates into O_2 and H_2O. MnO_2 can be ruled out as catalyst for O_2 formation at short reaction times because of its negligible activity in this solvent compared to that observed for the present complexes and the lack of a lag period corresponding to MnO_2 formation.

Kinetics. The initial rates of oxygen production for the H_2O_2 disproportionation reactions in methanol and dmf were measured in excess H_2O_2 and at constant temperature, for different concentrations of catalyst and H_2O_2. At constant [H_2O_2], the initial rate shows a linear dependence with the [catalyst] (Fig. S3†) and the first-order rate constant (k) was obtained from the slope of the line (Table 2). At constant [catalyst], **1** and **2** exhibit saturation kinetics with [H_2O_2] (Fig. 7) and the experimental data can be fitted to the Michaelis–Menten equation from which the catalytic turnover number (k_{cat}) and the Michaelis constant (K_M) were determined. Values of k_{cat} and K_M obtained for complexes **1** and **2** at 25 °C in methanol and dmf are listed in Table 3.

EPR and UV-VIS spectroscopies. The EPR spectra of **1** and **2** recorded in frozen dmf or methanol at various times following the addition of H_2O_2 exclude the formation of mixed-valence

Table 2 First-order rate constants independent of the [catalyst] at 25 °C

Complex	k/s^{-1}	Solvent	[H_2O_2]/mM
1	0.59(2)	Methanol	30
2	1.19(2)	Methanol	30
1	0.86(1)	dmf	55
2	1.43(2)	dmf	55

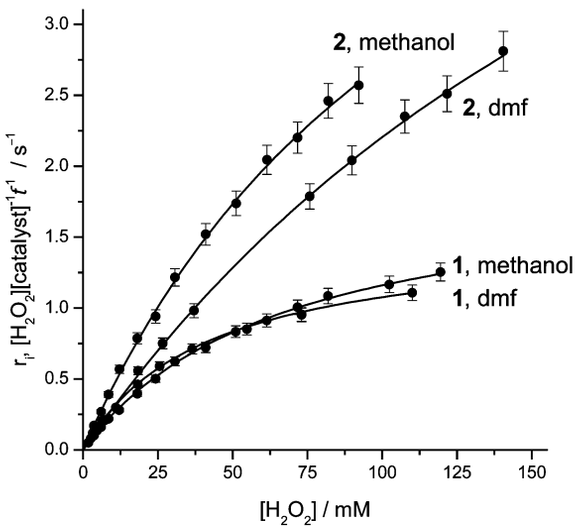

Fig. 7 Effect of the [H_2O_2] on the initial rate of H_2O_2 disproportionation at 25 °C, in methanol and dmf. [**1**] = 45 μM; [**2**] = 35 μM.

intermediates, either $Mn_2^{II,III}$ or $Mn_2^{III,IV}$ species, as these give rise to distinct, intense signals. Indeed, an EPR signal at $g \approx 2$ is detected, with five weak doublets ($\Delta m = 1$ nuclear-spin-forbidden transition)[39] inserted between the six absorptions characteristic of the hyperfine structure of an uncoupled Mn^{II} ion. This EPR signal does not disappear at the end of the reaction and can not be restored reversibly with more H_2O_2, indicating an irreversible decomposition product, and not an intermediate species. This Mn^{II} species forms at a much slower rate in dmf than in methanol. Addition of acid accelerates the apparition of the Mn^{II} signal, suggesting that formation of this uncoupled Mn^{II} species requires protons.

Room-temperature UV-VIS absorption spectra were taken during the progress of the reaction of complex **1** and **2** with H_2O_2 in methanol and dmf. When H_2O_2 is added to the catalyst in methanol, the green solution turns brown concomitantly with an increase in and a slight blue shift of the absorption bands (Fig. S4 †). For 50 : 1 or 100 : 1 H_2O_2 to catalyst ratios, the initial spectral pattern of **1** and **2** is restored after completion of the reaction but the intensity is lower than for the starting complex. When an excess larger than 200 : 1 of H_2O_2 over the catalyst is employed, the Mn^{III} spectral pattern is lost.

In dmf, upon addition of excess H_2O_2 over catalyst, an orange solution is generated within minutes, exhibiting an absorption maximum at 480 nm for **1** and 505 nm for **2**. Under conditions of saturating substrate concentration, this is the major species in solution (Fig. S5 †). As the colour of the solution changes to pink, the intensity of this band diminishes and a multiplet appears centred at $\lambda = 530$ nm on which vibrational fine structure separated by *ca.* 20 nm are superimposed. The multiline signal reaches a maximum corresponding to the steady state and then rapidly disappears, when the oxygen evolution ceases.

Discussion

The dismutation of H_2O_2 by complexes **1** and **2** shows saturation kinetics with substrate, first order dependence of the reaction rate on catalyst and proceeds without an initial time-lag. ^{1}H NMR experiments show that complex **1** retains dinuclearity during cycling as the signal of the aromatic proton appears unaltered at the end of the reaction. These experiments also reveal that, in methanol, the bridging acetate is retained during the catalysis, but acetate dissociates or shifts to a monodentate co-ordinated acetate in dmf. These observations indicate that **1** and **2** are responsible for the H_2O_2 disproportionation reaction, and suggest that H_2O_2 binds to these complexes in the first step by displacement of bound solvent.

Table 3 Kinetic parameters based on fits of the Michaelis–Menten equation to the rate data at 25 °C

Complex	k_{cat}/s^{-1}	10 K_M/mM	$k_{cat}K_M^{-1}$/M^{-1} s^{-1}	Solvent
1	2.0(1)	7.1(4)	28	Methanol
2	6.2(2)	13(2)	48	Methanol
3[a]	0.98(9)	1.4(5)	70	Methanol
4[a]	0.66(6)	3.6(3)	18	Methanol
1	1.6(2)	4.4(3)	36	dmf
2	7.9(3)	25(2)	32	dmf

[a] Data from ref. 15.

In dmf, the band at 480 nm observed in the dismutation of H_2O_2 by **1**, and 505 nm in the reaction with **2**, may account for the formation of a catalyst–substrate complex in rapid equilibrium with the unbound substrate. This is consistent with the increase of the maximal intensity of this band with increasing [H_2O_2], and with the fact that **2** requires an excess of H_2O_2 over catalyst larger than **1** to attain the maximal intensity of this band ($K_{M,3\text{-}OMe} > K_{M,5\text{-}OMe}$). In this solvent, the electronic spectra of the reaction of H_2O_2 with the two catalysts, show the growth and decay of a multiplet centred at 530 nm. Apparition and disappearance of such a multiplet had also been observed in H_2O_2 dismutation by complexes **3** and **4**.[15] The fine structure of this signal may be assigned to $\nu_{Mn=O}$ vibration coupled to a ligand-to-metal-charge-transfer band from O^{2-} to manganese in a high oxidation state through vibronic interactions.[40] This suggests that an oxidised oxo-manganese species is involved as an active species in the H_2O_2 disproportionation by **1**–**4**. A band at 530 nm with vibrational fine structure had previously been observed in the disproportionation of H_2O_2 by Mn^{II} dimers with phenolate-dicarboxylate[40–43] and pyrazolate-carboxylate[44] bridging cores and was attributed to the formation of the $[Mn^{IV}{=}O]_2$ species in a mechanism involving redox cycling between Mn_2^{III} and $[Mn^{IV}{=}O]_2$.

The number of equiv. of H_2O_2 that catalysts **1** and **2** may disproportionate is larger in dmf than in methanol. In the latter solvent, complexes **1** and **2** lose activity after 200 turnovers, Mn^{2+} accumulates in the reaction mixture – as evidenced by the growth of an EPR signal typical of uncoupled Mn^{2+} – and the [catalyst] in the solution decreases with the increasing number of cycles, as revealed by ^{1}H NMR and UV-VIS spectroscopies. Decomposition is observed to a lesser extent for **4** and is essentially absent in the case of **3**. Unlike in methanol, in dmf catalysts **1** and **2** disproportionate more than 1500 equiv. of H_2O_2 with only slight reduction of activity. Thus, protons must play an important role in the catalyst decomposition, which is favoured in protic solvents and accelerated by addition of acid to the reaction mixture.

Complexes **1**–**4** are isostructural, possess Mn ··· Mn distances around 2.93–2.94 Å and show the same magnetic behaviour. Electronic and ^{1}H NMR spectroscopies show that the four complexes are stable in methanol and dmf, even in the presence of water, and the NMR spectra reveal that the solid state structure of these complexes is retained in solution. Although the substituent, either *ortho* or *para* to the co-ordinate phenolate, does not affect the structure of the complexes in this series, they affect their redox potential and,

in consequence, their catalytic activity. The kinetic parameters of the four complexes are listed in Table 3. Complexes **1** and **2**, with an electron-donating substituent (MeO), are easier to oxidise (Fig. 4) and have higher maximal rates than the unsubstituted or the 5-Br substituted derivatives. The observed trend for the rates (MeO > H > Br) indicates that H_2O_2 reduction with concomitant oxidation of the catalyst should be the slow step in the catalytic cycle (the catalyst which is easier to oxidise reacts faster). In particular, the 3-MeO derivative has a k_{cat} value higher than expected from its oxidation potential. This seems to indicate some kind of participation of the *o*-MeO to facilitate the H_2O_2 reduction.

On the other hand, **3** and **4** have lower K_M values than the MeO derivatives, indicating that **1** and **2** are less efficient at binding the H_2O_2 substrate. Thus, although the MeO derivatives are more effective at reducing H_2O_2 they have difficulty in binding the substrate so that maximal rates can only be achieved at higher $[H_2O_2]$ than for **3** and **4**. This is especially evident for **2**, where the 3-MeO substituent, *ortho* to the coordinated phenolate, probably hampers the substrate approach toward the dimanganese centre.

EPR measurements exclude mixed valence Mn_2 complexes, so we think that the redox cycle should involve either a Mn_2^{II}/Mn_2^{III} or Mn_2^{III}/Mn_2^{IV} couple. Complexes **1** and **2** are EPR silent, so no EPR signal is expected for the catalyst occurring in the Mn_2^{III} oxidation state during cycling. The absence of an EPR signal during the reaction course – except for the inactive uncoupled Mn^{II} species – the lack of observation of Mn oxidation states different from Mn^{III} in the electronic spectra taken in methanol, the band at 480 (or 505) nm observed in dmf, typical of a high-valence Mn complex, together with the observation of the band at 530 nm with vibrational fine structure attributed to the formation of an oxidised oxo-manganese species, suggest that complexes of this series dismutate H_2O_2 by a mechanism involving redox cycling between Mn_2^{III} and Mn_2^{IV}. The fact that the oxidised and reduced Mn_2 species are observed in dmf but only the Mn_2^{III} species is detected in methanol may be interpreted as the consequence of the relative k_{ox} and k_{red} values in the two solvents. The k_{cat} trend for these complexes indicate that the oxidation of the catalyst (k_{ox}) is the slow reaction step ($k_{ox} < k_{red}$). Since for each complex the k_{cat} values (and thus the k_{ox}) are similar in both solvents, the observation of the oxidised species should reflect a k_{red} lower in dmf than in methanol.

In conclusion, although the electron-donating substituents in **1** and **2** improve the turnover rate of H_2O_2 dismutation, their low affinity for binding the substrate places the unsubstituted complex (**3**) as the most efficient (with optimal k_{cat}/K_M ratio) and stable (no significant decomposition is observed when more than 1000 equiv. of H_2O_2 are disproportionated) member of the series.

Experimental

Materials

All reagents or AR chemicals were used as purchased. Solvents were purified by standard methods. The concentration of H_2O_2 stock solution was determined by iodimetric titration. NaOMe solutions used in ^{1}H NMR experiments were prepared by dissolving Na in d_4-methanol.

Synthesis of ligands

5-MeO-salpentOH and 3-MeO-salpentOH were prepared by Schiff-base condensation of 1,5-diaminopentan-3-ol[45] with the corresponding aldehyde. 5-MeO-salpentOH was isolated by precipitation from the reaction mixture (ethanol) as a pure yellow solid (85%). 3-MeO-salpentOH precipitates as the sodium salt after addition of diethyl ether in the presence of excess NaOEt, to yield a pure yellow solid (39%). The two ligands were characterised by elemental analyses and ^{1}H NMR and IR spectroscopies.

Synthesis of catalysts

$[Mn_2(X\text{-salpentO})(\mu\text{-MeO})(\mu\text{-AcO})(MeOH)_2]Br$ (**1**: X = 5-MeO; **2**: X = 3-MeO) were obtained as green powders in 79% (**1**) and 71% (**2**) yield, following the procedure described in ref. 15 for **3** and **4**. Calculated for $Mn_2C_{26}H_{37}N_2O_{10}Br$: 42.9 C, 5.13 H, 3.85 N, 15.1 Mn. Found for **1**: 42.6 C, 5.30 H, 3.98 N, 15.3% Mn. IR (ν cm^{-1}): ν_{OH} 3349, $\nu_{C=N}$ 1625 (st), ν_{CO2} 1546/1417. UV-VIS λ_{max}/nm (ε/M^{-1} cm^{-1}) methanol: 336 (sh), 410 (6315), 663 (461); dmf: 405 (6000). Found for **2**: 42.8 C, 4.98 H, 4.03 N, 15.2% Mn. IR (ν cm^{-1}): ν_{OH} 3392, $\nu_{C=N}$ 1614 (st), ν_{CO2} 1551/1414. UV-VIS λ_{max}/nm (ε/M^{-1} cm^{-1}) methanol: 289 (24200), 393 (5953), 630 (544); dmf: 389 (4870). These absorbance bands obey Beer's law over the range of concentrations above 10 μM used in this work. Single crystals of **2** suitable for X-ray diffraction were obtained by crystallization from methanol upon standing in air for several days. Complexes **1** and **2** are stable in solution as revealed by the electronic, ^{1}H NMR and EPR spectra of the complexes recorded at different time-lengths after the preparation of the solutions in anhydrous dmf and methanol, or following water addition (up to 10%).

Physical measurements

Variable-temperature magnetic susceptibility data were obtained with a Quantum Design MPMS SQUID susceptometer, under a magnetic field of 1 T in the temperature range 4–300 K. Diamagnetic corrections were applied by using Pascal's constants. Least-squares computer fitting of the data was accomplished with a function-minimization program. Instruments and conditions for IR, EPR, UV-VIS, electrochemical, initial rate and volumetric measurements are the same as those described in ref. 15.

^{1}H NMR measurements

Solutions of the Mn complexes in d_4-MeOH or d_7-dmf were prepared in order to record the ^{1}H spectra on a Bruker AC 200 NMR spectrometer at ambient probe temperature (*ca.* 26 °C). The nominal operating frequencies were 200.1 and 50.3 MHz. A super-weft pulse sequence for intense water suppression in paramagnetic samples[46] was used whenever water needed to be added to the sample. In each case the D1 (τ) value in the weft sequence was selected from an inversion–recovery T1 experiment with delay list cycling (Bruker standard software) such as to provide maximum water suppression. For the paramagnetic samples, typically operation conditions were: 400 to 500 transients, recycle delay 0.5 s, acquisition time 0.65 s and a SW of 25000 Hz (124.9 ppm). D1 (τ) were typically between 0.00184 and 0.024 s.

X-Ray crystal structure determination

The pertinent crystallographic data together with the refinement details for $[Mn_2(3\text{-OMe-salpentO})(\mu\text{-MeO})(\mu\text{-AcO})(MeOH)_2]Br$ (**2**) are summarized in Table 4.

The crystal data were collected at 293 K on an Enraf-Nonius CAD4 diffractometer using graphite-monochromated Mo-Kα radiation (λ = 0.71073 Å). Data reduction was made with the MolEN package.[47] Absorption corrections from psi scans were applied (maximum and minimum transmission factors = 0.9995–0.8380).[48]

The structure was solved by direct methods using SHELXS-97[49] and refined on F^2 by full-matrix least-squares using SHELXL-97[50] with anisotropic displacement parameters for all non-hydrogen atoms. Hydrogen atoms bonded to O(7) and O(8) atoms were refined isotropically. The other H atoms were introduced in calculations using the riding model with isotropic thermal parameters 1.1 times higher than those of the atom to

Table 4 Crystal data and structure refinement for $[Mn_2(3\text{-OMe-salpentO})(\mu\text{-MeO})(\mu\text{-AcO})(MeOH)_2]Br$ (**2**)

Formula	$C_{26}H_{37}BrMn_2N_2O_{10}$
Formula weight	727.37
Crystal dimensions/mm	0.50 × 0.20 × 0.15
Crystal system	Monoclinic
Space group	$P2_1/n$ (no. 14)
a/Å	13.6590(17)
b/Å	16.8728(16)
c/Å	14.2528(18)
β/°	112.020(11)
V/Å^3	3045.2(6)
Z	4
F(000)	1488
T/K	293
D_c/Mg m^{-3}	1.587
μ(Mo-Kα)/mm^{-1}	2.197
No. collected reflections	6211
No. unique reflections	5975 [Rint = 0.0225]
No. of observed reflections	3646
No. of refined parameters	378
$wR(F^2)$	0.0580
$R[F > 4\sigma(F)]$	0.0310
Goodness-of-fit on F^2	0.956
($\Delta\rho$) max, min/e Å^{-3}	0.287, −0.431

which they are bonded. Scattering factors were taken from ref. 51. The molecular plot was obtained using the ZORTEP[52] program.

CCDC reference number 185611.

See http://www.rsc.org/suppdata/dt/b2/b204566d for crystallographic data in CIF or other electronic format.

Acknowledgements

We thank the National Research Council of Argentina (CONICET), the National University of Rosario, Antorchas Foundation, the TWAS and the National Agency for Sciences Promotion for financial support. We thank Mónica de Gaudio for the volumetric measurements.

References

1 V. L. Pecoraro (Editor), *Manganese Redox Enzymes*, VCH, New York, 1992.
2 Y. Kono and I. Fridovich, *J. Biol. Chem.*, 1983, **258**, 6015–6019.
3 Y. Kono, *J. Biol. Chem*, 1983, **258**, 13646–13648.
4 V. V. Barynin and A. Grebenko, *Dokl. Akad. Nauk. SSSR*, 1986, **286**, 461–464.
5 G. S. Allgood and J. J. Perry, *J. Bacteriol.*, 1986, **168**, 563–567.
6 D. W. Yoder, J. Hwang and J. E. Penner-Hahn, in *Metal Ions in Biological Systems: Manganese and its Role in Biological Processes*, eds. A. Sigel and H. Sigel, Marcel Dekker Inc., New York, vol. 37, 2000, pp. 527–557.
7 P. J. Riggs-Gelasco, R. Mei and J. E. Penner-Hahn, in *Mechanistic Bioinorganic Chemistry*, eds. H. H. Thorp and V. L. Pecoraro, American Chemical Society, Washington, DC, 1995, pp. 219–248.
8 J. E. Penner-Hahn and V. L. Pecoraro, in *Manganese Redox Enzymes*, ed. V. L. Pecoraro, VCH, New York, 1992, pp. 29–45.
9 I. Michaud-Soret, L. Jacquamet, N. Debaecker-Petit, L. Le Pape, V. V. Barynin and J.-M. Latour, *Inorg. Chem.*, 1998, **37**, 3874–3876.
10 V. L. Pecoraro and W.-Y. Hsieh, in *Metal Ions in Biological Systems: Manganese and its Role in Biological Processes*; eds. A. Sigel and H. Sigel, Marcel Dekker Inc., New York, vol. 37, 2000, pp. 431–444.
11 V. L. Pecoraro, M. J. Baldwin and A. Gelasco, *Chem. Rev.*, 1994, **94**, 807–826.
12 N. N. Gerasimchuk, A. Gerges, T. Clifford, A. Danby and K. Bowman-James, *Inorg. Chem.*, 1999, **38**, 5633–5636.
13 S. J. Brudenell, L. Spiccia, A. M. Bond, G. D. Fallon, D. C. R. Hockless, G. Lazarev, P. J. Mahon and E. R. T. Tiekink, *Inorg. Chem.*, 2000, **39**, 881–892.
14 M. Maneiro, M. R. Bermejo, A. Sousa, M. Fondo, A. M. González, A. Sousa-Pedrares and C. A. McAuliffe, *Polyhedron*, 2000, **19**, 47–54.
15 C. Palopoli, B. Chansou, J. P. Tuchagues and S. Signorella, *Inorg. Chem.*, 2000, **39**, 1458–1462.
16 T. Nakamura, K. Niwa, S. Usugi, H. Asada, M. Fujiware and T. Matsushita, *Polyhedron*, 2001, **20**, 191–201.
17 M. McCoy, *Chem. Eng. News*, 1999, **77**, 18–19.
18 R. Hage, J. E. Iburg, J. Kerschner, J. H. Koek, E. L. M. Lempers, R. J. Martens, U. S. Racheria, S. W. Russell, T. Swarthoff, M. R. P. van Vliet, J. B. Warnaar, L. van der Wolf and B. Krijnen, *Nature (London)*, 1994, **369**, 637–639.
19 J. Brinksma, R. Hage, J. Kerschner and B. L. Feringa, *Chem. Commun.*, 2000, 537–538.
20 A. E. M. Boelrijk and G. C. Dismukes, *Inorg. Chem.*, 2000, **39**, 3020–3028.
21 P. J. Pessiki and G. C. Dismukes, *J. Am. Chem. Soc.*, 1994, **116**, 898–903.
22 A. Gelasco, S. Bensiek and V. L. Pecoraro, *Inorg. Chem.*, 1998, **37**, 3301–3309.
23 A. Gelasco, M. L. Kirk, J. W. Kampf and V. L. Pecoraro, *Inorg. Chem.*, 1997, **36**, 1829–1837.
24 M. Mikuriya, Y. Yamato and T. Tokii, *Bull. Chem. Soc. Jpn.*, 1992, **65**, 2624–2637.
25 Z. Zhang, C. Brouca-Cabarrecq, C. Hemmert, F. Dahan and J. P. Tuchagues, *J. Chem. Soc., Dalton Trans.*, 1995, 1453–1460.
26 C. J. O'Connor, *Prog. Inorg. Chem.*, 1982, **29**, 203–283.
27 Y. Nishida, N. Oshino and T. Tokii, *Z. Naturforsch., Teil B*, 1988, **43**, 472–474.
28 E. A. Lewis, J. R. Lindsay Smith, P. H. Walton, S. J. Archibald, S. P. Foxon and G. M. P. Giblin, *J. Chem. Soc., Dalton Trans.*, 2001, 1159–1161.
29 J. Bonadies, M. Maroney and V. L. Pecoraro, *Inorg. Chem.*, 1989, **28**, 2044–2051.
30 M. T. Caudle, P. Riggs-Gelasco, A. K. Gelasco, J. E. Penner-Hahn and V. L. Pecoraro, *Inorg. Chem.*, 1996, **35**, 3577–3584.
31 M. R. Bermejo, A. M. González, M. Fondo, A. García-Deibe, M. Maneiro, J. Sanmartín, O. Hoyos and M. Watkinson, *New J. Chem.*, 2000, **24**, 235–241.
32 D. W. Wright, H. J. Mok, C. E. Dubé and W. H. Armstrong, *Inorg. Chem.*, 1998, **37**, 3714–3718.
33 R. Hage, E. A. Gunnewegh, J. Niël, F. S. B. Tjan, T. Weyhermüller and K. Weighardt, *Inorg. Chim. Acta*, 1998, **268**, 43–48.
34 A. E. M. Boelrijk, S. V. Khangulov and G. C. Dismukes, *Inorg. Chem.*, 2000, **39**, 3009–3019.
35 E. J. Larson and V. L. Pecoraro, *J. Am. Chem. Soc.*, 1991, **113**, 7809–7810.
36 J. Bonadies, M. Kirk, M. Lah, D. Kessissoglou, W. Hatfield and V. L. Pecoraro, *Inorg. Chem.*, 1989, **28**, 2037–2044.
37 E. J. Larson and V. L. Pecoraro, *J. Am. Chem. Soc.*, 1991, **113**, 3810–3818.
38 B. Albela, G. Chottard and J. J Girerd, *J. Biol. Inorg. Chem.*, 2001, **6**, 430–434.
39 B. Bleaney and R. S. Rubins, *Proc. Phys. Soc., London*, 1961, **77**, 103–112.
40 H. Sakiyama, H. Okawa and R. Isobe, *J. Chem. Soc., Chem. Commun.*, 1993, 882–884.
41 H. Sakiyama, H. Tamaki, M. Kodera, N. Matsumoto and H. Okawa, *J. Chem. Soc., Dalton Trans.*, 1993, 591–595.
42 C. Higuchi, H. Sakiyama, H. Okawa and D. Fenton, *J. Chem. Soc., Dalton Trans*, 1995, 4015–4020.
43 T. Aono, H. Wada, M. Yonemura, M. Ohba, H. Okawa and D. Fenton, *J. Chem. Soc., Dalton Trans.*, 1997, 1527–1531.
44 M. Itoh, K. Motoda, K. Shindo, T. Kamiusuki, H. Sakiyama, N. Matsumoto and H. Okawa, *J. Chem. Soc., Dalton Trans.*, 1995, 3635–3641.
45 I. Murase, M. Hatano, M. Tanaka, S. Ueno, H. Okawa and S. Kida, *Bull. Chem. Soc. Jpn.*, 1982, **55**, 2404–2408.
46 T. Inubushi and E. D. Becker, *J. Magn. Reson.*, 1983, **51**, 128.
47 C. K. Fair, Mo1EN, Structure solution procedures, Enraf-Nonius, Delft, Holland, 1990.
48 A. C. T. North, D. C. Phillips and F. S. Mathews, *Acta Crystallogr., Sect. A*, 1968, **24**, 351–359.
49 G. M. Sheldrick, SHELXS-97, Program for Crystal Structure Solution, University of Göttingen, Göttingen, Germany, 1990.
50 G. M. Sheldrick, SHELXL-97, Program for the refinement of crystal structures from diffraction data, University Göttingen, Göttingen, Germany, 1997.
51 *International Tables for Crystallography*, Kluwer Academic Publishers, Dordrecht, The Netherlands, vol. C, 1992, Tables 4.2.6.8 and 6.1.1.4.
52 L. Zsolnai, H. Pritzkow and G. Huttner, ZORTEP, Ortep for PC, Program for Molecular Graphics, University of Heidelberg, Heidelberg, Germany, 1996.